Eur. Phys. J. B **35**, 481–491 (2003)
DOI: 10.1140/epjb/e2003-00301-6

THE EUROPEAN PHYSICAL JOURNAL B

Effects of vacuum annealing on the transport property of $La_{0.67}Sr_{0.33}MnO_{3-\delta}$ films

J.R. Sun[1,2,a], H.W. Yeung[2], H.K. Wong[2], T. Zhu[1], and B.G. Shen[1]

[1] State Key Laboratory for Magnetism, Institute of Physics and Center for Condensed Matter Physics, The Chinese Academy of Sciences, Beijing 100080, P.R. China
[2] Department of Physics, The Chinese University of Hong Kong, Hong Kong, P.R. China

Received 11 April 2003 / Received in final form 8 August 2003
Published online 24 October 2003 –

Abstract. Effects of oxygen content on the transport behavior of epitaxial $La_{2/3}Sr_{1/3}MnO_{3-\delta}$ films on (110) $NdGaO_3$ and (001) $SrTiO_3$ substrates have been experimentally studied. A quantitative relation between the temperature of metal-to-insulator transition (T_p) and the content of oxygen vacancies is established, and it is found that oxygen non-stoichiometry causes a monotonic decrease of T_p. A comparison to crystals $La_{1-x}Sr_xMnO_3$ indicates that the reduction of hole concentration due to the incorporation of anionic vacancies dominates the variation of T_p, while the vacancies themselves influence the detailed features of the T_p-δ dependence. Strain in the film affects the effects of oxygen deficiency, and the metal-to-insulator transition disappears at a smaller δ value in tensily stressed films. In the temperature region above T_p, oxygen vacancies affect the resistive behavior of the films mainly by modulating the content of Mn^{4+}. In contrast, extra effects due to the scattering of oxygen vacancies become important at low temperatures, causing an exponential increase of resistivity with δ. A further analysis indicates that oxygen deficiency enhances magnetic scattering, and leads to a resistivity upturn of the form $-\ln(T)$ when δ is significant.

PACS. 75.30.-m Intrinsic properties of magnetically ordered materials – 73.50.-h Electronic transport phenomena in thin films – 68.60.-p Physical properties of thin films, nonelectronic

1 Introduction

Effects of oxygen non-stoichiometry in the manganite $La_{1-x}A_xMnO_3$ (A: divalent ions) have received a wide attention since the discovery of colossal magnetoresistance (CMR) in this kind of materials [1]. According to the double exchange (DE) theory [2], e_g electrons can hop between Mn^{3+} and Mn^{4+} ions under the help of intermediate oxygen while retaining their spin orientations, which produces a magnetic coupling among Mn ions. The transfer rate for the electron is proportional to $\cos(\theta/2)$, where θ is the angle between two adjacent spins. Therefore, the depression of spin fluctuation by an applied field or by a paramagnetic to ferromagnetic transition will cause an enhancement of conduction. In this picture, the CMR effects and why metallic conduction always occurs below Curie temperature can be understood qualitatively. It is obvious that oxygen vacancies will affect the contents of Mn^{3+} and Mn^{4+}, which are the principal ingredient for the DE, yield lattice distortion/disorder and break the bridge for the charge exchange. All these are expected to have a strong impact on the property of the materials.

In fact, attempts to elucidate the role of oxygen have never stopped since the discovery of the novel magnetic and transport properties of the manganites by Jonker and Van Santen [3]. The earliest work may be that of Yekal [4]. In a paper published in 1955, he tried to establish a universal relation between crystal structure and the content of Mn^{4+} by doping divalent ions into the La-site or by introducing vacancies into the oxygen sublattice. This work revealed an expansion of lattice and a degeneration of structure symmetry with the incorporation of oxygen vacancies, which are the general features of the effects of oxygen deficiency on structure as confirmed by subsequent researches. A further study was given recently by Mittchel et al. [5] and Huang et al. [6]. Using neutron diffraction, combined with the Rietveld data analysis technique, the authors can determine the crystal structure and the oxygen content simultaneously. They observed a tetrahedral to monoclinic structure transition after significant oxygen loss. It is obvious that oxygen non-stoichiometry will affect not only the structure of the manganites but also their

[a] e-mail: jrsun@g203.iphy.ac.cn

magnetoresistive properties. Ju and co-workers [7] reported a reduction in magnetization and Curie temperature and an increase in resistivity and magnetoresistance in oxygen-deficient $La_{0.7}Ba_{0.3}MnO_3$. Meanwhile, the fully spin-aligned state becomes hard to reach even at low temperatures. Essentially similar phenomena were observed by Léon-Guevara et al. [8] in single crystal $La_{1-x}Sr_xMnO_{3-\delta}$ and by Krishnan et al. [9] and Liu et al. [10] in manganite thin films.

Now it is generally believed that the effects of oxygen deficiency duplicate all the salient features of divalent ion-doping. However, the lattice defects in this case may also have a strong impact on the magnetic and transport properties of the manganites taking into account that oxygen vacancies can block the DE path of the e_g electrons like the secondary ions at Mn-site [11]. Therefore, it is a reasonable expectation that considerable difference can exist between the effects of oxygen deficiency and divalent doping. A quantitative study can be helpful for the identification of these effects noting that hole-concentration and lattice defects may work independently in the DE process. Because of the difficulty of the precise determination of the oxygen content, unfortunately, most of the known investigations provided a qualitative picture of the oxygen effects. Though Ju et al. [7], Léon-Guevara et al. [8], and Malavasi et al. [12] have tried to measure the content of oxygen, the detailed dependence of resistivity on temperature and oxygen content was not given, and the possible extra effects associated with oxygen vacancies were not analyzed either. Moreover, their researches were performed for bulk manganites, for which inhomogeneous oxygen distribution is possible when the samples are treated under various atmospheres to tune their oxygen content [13].

There are two differences between bulk materials and thin films. The first one is that the surface-to-volume ratio is large in the latter, which makes it is easy to remove or insert an oxygen from or into the oxygen sublattice. The second difference is that the strain in the film can be artificially controlled. Obviously, a quantitative study in this case is more difficult since the sophisticated techniques such as chemical titration and thermogravimetry for the determination of oxygen content can not be utilized. To avoid the difficulty of determining oxygen content, as an alternative, people usually prepared or post-annealed the film under different oxygen partial pressures [10]. Though this procedure gives a systematic variation, a quantitative relation cannot be gained in this way.

In this paper, we present a comprehensive study on oxygen effects in $La_{0.67}Sr_{0.33}MnO_{3-\delta}$ thin films via measuring oxygen deficiency by lattice constant. Special attention was paid to the quantitative relation between transport property and oxygen content, and the difference between the effects of oxygen non-stoichiometry and Sr-doping. It is found that the behavior of vacuum-annealed film mimics in general that of the bulk $La_{1-x}Sr_xMnO_3$ with various Sr contents. We observed a monotonic decrease of the critical temperature for the metal-to-insulator (M-I) transition and an enhancement of resistivity with the decrease of oxygen content. Compared with the bulk materials, however, the M-I transition in oxygen-deficient film is broader and more ambiguous, and the transition temperature is also lower. Furthermore, the presence of oxygen vacancies affects the residual resistivity strongly, causing an exponential increase of the resistivity with vacancy concentration. The arrangements of this paper are as follows: The next section is a simple description of the experiment procedure. The mains results are presented in Section 3, in which the effects of oxygen deficiency on structure, transport property, and M-I transition are studied and compared to bulk $La_{1-x}Sr_xMnO_3$ with similar hole concentrations. The last section gives a simple summary.

2 Experiment

Two $La_{0.67}Sr_{0.33}MnO_{3-\delta}$ films respectively on (001) $SrTiO_3$ (LSMO/STO) and (110) $NdGaO_3$ (LSMO/NGO) substrates were prepared from the stoichiometric targets using a facing-target sputtering technique [14]. To eliminate undesired extra effects, the two substrates with the same size of 8×1 mm^2 were placed side by side on sample holder. The substrate temperature was kept at 710 °C and the O_2 partial pressure at 30 mTorr during the deposition. The film thickness was ∼1500 Å, controlled by sputtering time with the deposition rate (0.32 Å/s) being carefully calibrated. To improve oxygen stoichiometry, the resulting samples were annealed at 900 °C in O_2 atmosphere of 1 bar for 4 hours. Samples thus obtained (called as-prepared hereafter) should be oxygen stoichiometric (δ=0) for that a further annealing has minor effects on the temperature for the M-I transition.

The surface morphology of the LSMO film was studied by Atomic Force Microscopy (AFM), and the structure was analyzed with a Huber four-circle X-ray diffractometer using Cu K_α radiation. Resistance was measured by the conventional four-probe technique in the temperature range from 24 K to 300 K. Four rectangle-shaped silver pads with a space of 1 mm were evaporated on film surface to improve the electric contact and to eliminate the uncertainty of sample geometry that may influence the estimate of resistivity.

To remove oxygen, the two side by side placed films were heated at a rate of ∼200 °C/hour, in a vacuum of $\sim8\times10^{-7}$ Torr, to a predetermined temperature between 200−400 °C first, then cooled to room temperature. A lower temperature was set in the beginning of the treatment to control the release of oxygen. Further deprivation of oxygen requires higher temperatures when oxygen vacancies are significant. After each heating-cooling cycle, the (220)/(004) peak was recorded carefully, which gives the out-of-plane lattice parameter that has been used to characterize the oxygen content of the film, and the resistance as a function of temperature was measured. This process was repeated to trace the variation of oxygen content and resistivity. Similar studies were also performed for three $La_{0.67}Ca_{0.33}MnO_{3-\delta}$ (LCMO) films on STO, NGO and AlN(50Å)/STO, respectively (1500 Å in thickness and prepared following the same procedure as the LSMO

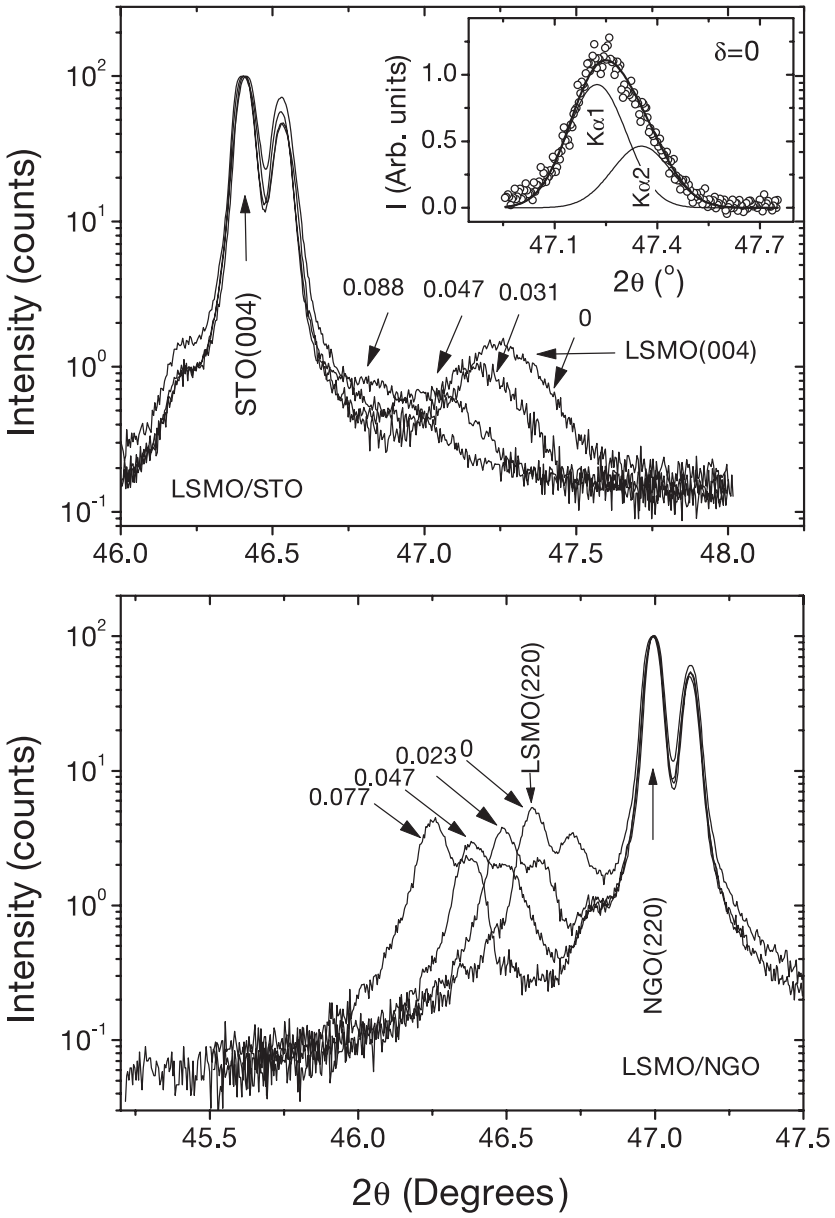

Fig. 1. X-ray diffraction patterns against vacuum annealing for the $La_{0.67}Sr_{0.33}MnO_{3-\delta}$ films on $SrTiO_3$ (top panel) and $NdGaO_3$ (bottom panel). The inset is a close view of the observed and calculated (004) peaks of LSMO/STO. Numbers in the Figure indicate the δ values of the corresponding spectra (see the context).

films). In the third film, a AlN buffer layer of 50 Å was sandwiched. It is found that the general features of the vacuum annealing effects are the same for the LSMO and LCMO films. Therefore, we mainly present the results for the LSMO system here.

3 Results and discussions

3.1 Oxygen release and its characterization

According to the AFM study, the film is smooth with a mean surface roughness of ∼40 Å, essentially independent of substrate. X-ray diffraction (XRD) study shows that both LSMO films are good epitaxial films, and only those peaks coherent with the substrate were detected. Figure 1 shows the XRD patterns of the as-prepared and vacuum-annealed LSMO films. For LSMO/NGO, the full width at half maximum (FWHM) of the (220) peak (the highest peak) is ∼0.1°, comparable to that of the NGO substrate (∼0.05°). $\phi-$scan of the same peak gives a FWHM of ∼0.1° for the film while ∼0.06° for the substrate (not shown). In contrast, the XRD peak of LSMO/STO is much broader, and the reflections of Cu K_{α_1} and K_{α_2} can not be distinguished from each other. Fitting the XRD peaks by two Gaussian functions, we

obtained FWHM≈0.18° (inset to Fig. 1), a width much wider than that of the $SrTiO_3$ substrate (∼0.062°).

The large film-substrate lattice mismatch may be the reason for the poor crystal quality of LSMO/STO. The lattice parameter is 3.8804 Å for bulk LSMO (For the sake of simplicity, all the lattice parameters given here are for the pseudo-cubic structure) and 3.905 Å for the STO crystal, then the lattice mismatch is ∼0.64%. In contrast, the lattice mismatch in LSMO/NGO is ∼0.38% (the lattice parameter is 3.8650 Å for NGO). This analysis is consistent with the experiment results. Taking the diffraction peak of the substrate as a reference, the out-of-plane lattice parameter of the film can be derived accurately from the XRD data. It gives $d = 3.8392$ Å and 3.8971 Å for the as-prepared LSMO/STO and LSMO/NGO. The former is smaller while the latter is larger than the bulk value (3.8804 Å), indicating a tensile stress in LSMO/STO and a compressive stress in LSMO/NGO. The quality of the substrate may be another factor affecting the film.

Annealing the film in high vacuum drives the XRD peak to lower 2θ angles. Take LSMO/NGO as an example. The (220) peak shifts from 46.588° to 46.08° after repeated vacuum annealing, indicating a lattice expansion of ∼1% in the direction normal to the film plane. Figure 2 presents the out-of-plane lattice parameters of the LSMO films (top panel). It shows a monotonic expansion of the lattice. The lattice constant grows from 3.8950 Å to 3.9362 Å for LSMO/NGO and from 3.8448 Å to 3.8831 Å for LSMO/STO. This result confirms the occurrence of oxygen release considering the fact that it will convert the smaller Mn^{4+} into larger Mn^{3+} to keep valence balance (the six-coordinate ionic radius is 0.53 Å for Mn^{4+} and 0.645 Å for Mn^{3+} according to Shannon [15]). Correspondingly, strain in the film changes conspicuously. In the ultimately oxygen-deficient LSMO/STO, for example, the lattice constant is 3.8831 Å, essentially the same as the bulk LSMO, which means that the film is nearly strain free or slightly tensily strained. In contrast, the compressive stress in LSMO/NGO is enhanced. A crucial observation is that the lattice parameter varies at a similar rate for the two films, as shown in the top panel of Figure 2. It is not a coincidence, but an indication that the oxygen release in both films is the same despite the different strains and crystal qualities of the films.

The key problem for a quantitative investigation of the effects of oxygen non-stoichiometry is the determination of oxygen content. Lattice parameter could be used for this purpose. For bulk materials, early experiment has revealed an expansion of unit cell with the concentration of oxygen vacancies [4,7]. For an epitaxial film, lattice expansion could take place mainly along the film normal since the lateral lattice has to match the substrate. On the analogy of the bulk manganites, the variation of oxygen content vs lattice constant is expected to be linear when it is not large, i.e., $\delta = \alpha \Delta d$, where Δd is the change of lattice parameter due to oxygen losing. We analyzed the data of the $La_{1-x}Sr_xMnO_3$ crystals, and found that the low temperature resistivity is much more sensitive to the content of oxygen compared with T_p [13]. Therefore, we

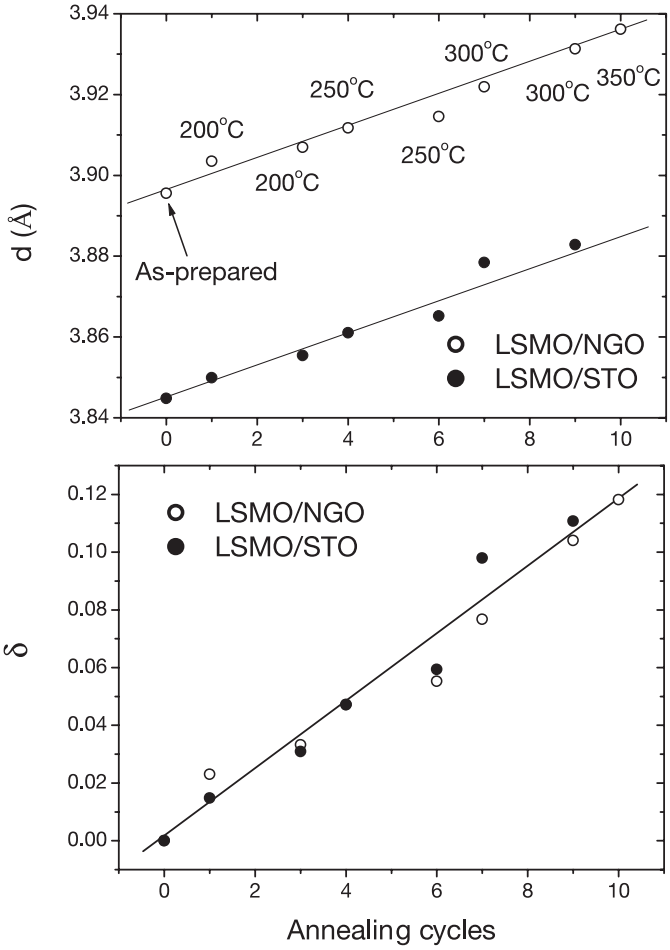

Fig. 2. Out-of-plane lattice parameters (top panel) and the content of oxygen vacancies (δ) (bottom panel) against the heating-cooling cycle. The preset temperature for each annealing cycle is marked by a label in the top panel. Solid lines are guides for the eye.

use it to calibrate the oxygen content in the LSMO films. A typical feature of the $\rho - x$ curve of $La_{1-x}Sr_xMnO_3$ is the presence of an obvious upturn at $x \approx 0.18$, below which the resistivity grows rapidly with the decrease of x [16]. A basic assumption for our calibration is that a similar feature should appear when the Mn^{4+} content is modulated by oxygen vacancy. As will be seen in the following section, this requirement can be met by setting δ to 0 for the as-prepared LSMO/NGO film and to 0.077 after 7 annealing cycles ($x = 1/3 - 2\delta \approx 0.18$). Regarding the lattice parameter of 3.8956 Å and 3.9219 Å in these two cases, it is easy to obtain $\delta = 2.864\Delta d$. Noting the accuracy of ∼0.0005 Å of lattice constant based on XRD, a variation of ∼0.002 in oxygen content can be reliably detected. Though the actual precision could be somewhat lower due to possible lattice relaxation, it is still enough to capture a tiny variation of oxygen content.

The bottom panel of Figure 2 presents the content of oxygen vacancies thus obtained. According to Figure 2,

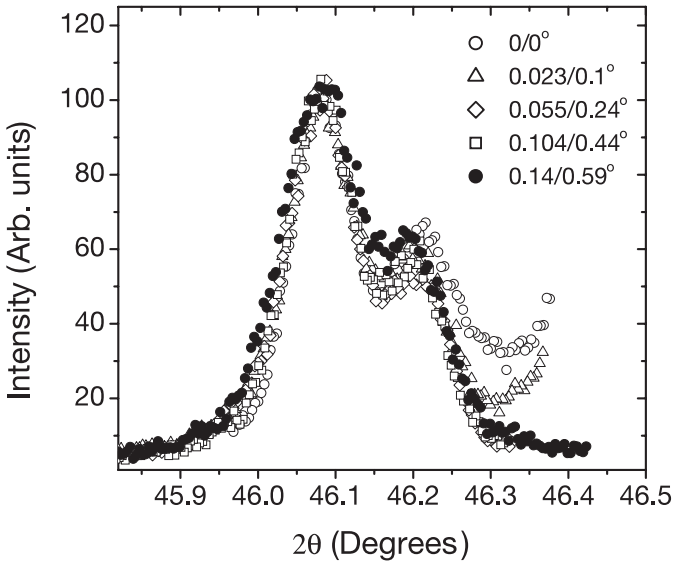

Fig. 3. X-ray diffraction patterns for LSMO/NGO at different stages of vacuum annealing. A shift in peak position [$\Delta(2\theta)$] and a renormalization in intensity were made for comparison. Labels in the figure are the values of $\delta/\Delta(2\theta)$.

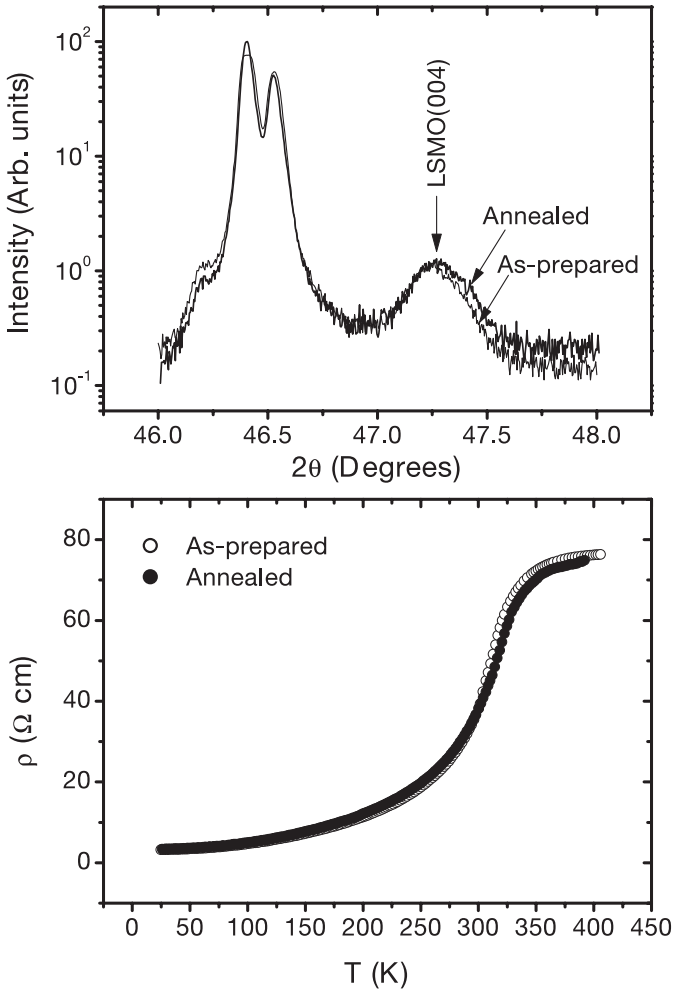

Fig. 4. X-ray diffraction spectra of the as-prepared and repeatedly annealed (in vacuum and in oxygen atmosphere) LSMO/NGO film (top panel) and the corresponding resistivity as a function of temperature.

significant oxygen losing occurs at 200 °C. This is a temperature much lower than that required by bulk LSMO, for which a minimum temperature for considerable oxygen release is ∼700 °C. The larger surface-to-volume ratio of thin films explains this difference. The presence of oxygen vacancies does not influence the crystal quality of the film significantly. Figure 3 illustrates the peak profiles of the (220) reflection of LSMO/NGO. It shows that the FWHM of (220) remains unchanged at different stages of the vacuum annealing (the slight broadening of the K_{α_2} peaks in the case of $\delta = 0$ and 0.023 is due to the contribution of substrate). Therefore, the effects associated with the random distribution of oxygen vacancies may be unimportant when the concentration of oxygen vacancies is small. However, irreversible peak broadening takes place for δ>0.14. In this case, a cooperative lattice distortion due to the incorporation of oxygen vacancies could occur.

After repeated vacuum annealing, the films were socked in 1 atm O_2 gas at 300 °C for 1 hour. It is found that with the restoration of the initial lattice constant, the original resistivity recovers simultaneously if the concentration of oxygen vacancies is not too large (Fig. 4). This result indicates that the effects of irreversible lattice relaxation and the intra- or interlayer atomic diffusion are negligible, which justifies the measurement of oxygen deficiency by Δd.

3.2 Transport property

Figure 5 presents the temperature dependence of the resistivity of LSMO, $\rho(T)$. For the as-prepared film, a typical metallic conduction is observed in the entire temperature range investigated. The resistivity decreases smoothly with cooling at first, then drops rapidly near $T_p \approx 350$ K, at which a paramagnetic to ferromagnetic transition takes place according to the bulk materials. After this transition, the gradual and smooth variation of resistivity recovers. The residual resistivity, extrapolated to 0 K, is $\sim 2\times10^{-4}$ Ω cm (slightly film-dependent), a value comparable to that of single crystals (denoted as LaSr) with similar Sr content (0.5×10^{-4} Ω cm) [16]. With the progress of oxygen release, the $\rho(T)$ curve above T_p flattens gradually and, finally, changes into a semiconductive conduction ($d\rho/dT$<0) when δ exceeds 0.015 (corresponding to $x = 1/3 - 2\delta \approx 0.3$). Accordingly, the overall resistivity increases, and a resistive upturn emerges and develops below ∼60 K. Accompanying with these, the critical temperature T_p, which delimits the metallic and the semiconductive behaviors, shifts to low temperatures, and the M-I transition broadens systematically.

These are results similar to those observed by other authors in oxygen-deficient films except for that the anionic vacancies are quantified in the present case, which allows

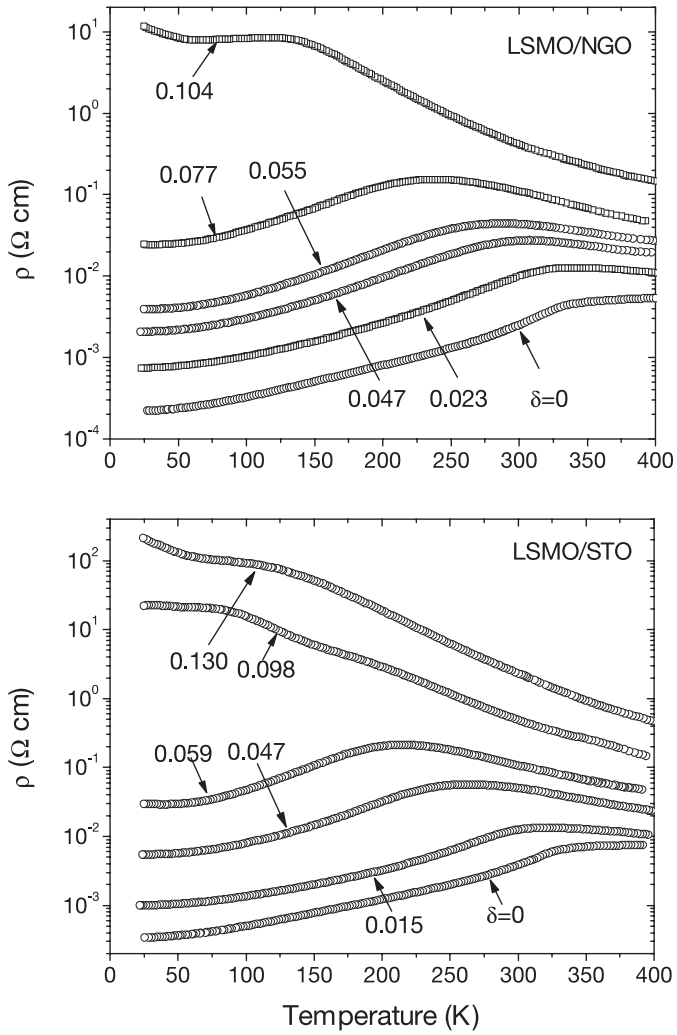

Fig. 5. Resistivity as a function of temperature for LSMO/NGO (top panel) and LSMO/STO (bottom panel). Numbers in the figure denote the δ values of the corresponding curves.

a quantitative study of the effect of oxygen deficiency on T_p and the $\rho - \delta/\rho - T$ relations. In Figure 6 (top panel) we show the resistivity as a function of δ at six selected temperatures between 25 K and 400 K. Results of LaSr are also presented for comparison. An approximately exponential increase of ρ with δ is observed for a large range of δ at all the temperatures. The $\ln(\rho) - \delta$ slopes can be classified into two definitely different groups, and they are ∼23.6 and ∼16 below and above T_p, respectively. The latter is obviously smaller. Similar results are obtained for LSMO/STO except for that the slope is a little different (inset in Fig. 6). The rapid increase of resistivity with oxygen deficiency is consistent with the dramatic reduction of magnetization. We have measured the hysteresis loop of LCMO/AlN/STO, and found that, in addition to a slow increase of coercivity, the magnetization at 5 K decreases from $\sim 3.6\ \mu_B$/Mn for $\delta = 0$ to $\sim 1\ \mu_B$/Mn for $\delta = 0.06$ (not shown).

Ordinarily, the reduction in the Mn^{4+} concentration will cause an increase of resistivity, but this change is rather smooth when x varies in the range 0.18–0.4 as shown by the results of the LaSr crystals (bottom panel in Fig. 6) [16,17]. The great difference between the LaSr crystals and the LSMO films may be an indication that other mechanisms are in play. Different from the former, the hole concentration in the latter is modified by oxygen vacancies instead of divalent ion. In this case, two extra factors disfavoring the electronic conduction are expected. First, La-site potential fluctuation due to the simultaneous presence of La^{3+} and Sr^{2+} remains large when the Mn^{4+} content reduces. Second, oxygen vacancy will affect the ferromagnetic coupling between Mn ions by breaking the Mn^{3+}-Mn^{4+} pair in addition to reducing the content of Mn^{4+}. The latter may be more important for that not only the Mn ions in the Mn-V-Mn chain (V denotes the oxygen vacancy) but also all the ions within a certain distance from the vacancy could be affected. In fact, though an anionic vacancy releases two electrons, the two electrons would be tied to the vacancy by electrostatic attraction. This reminds us of the halide, in which each anionic vacancy binds one electron, forming a color center [18]. It is noteworthy that the binding energy of the vacancies could be significant. Alonso and co-workers [19] have discussed the effects of Ga-doping on $La_{0.67}Ca_{0.33}MnO_3$, and pointed out that the electrostatic potential which binds the nearby Mn^{4+} ions to a Ga^{3+} ion is ∼0.5 eV. As a consequence, the Mn ions near an oxygen vacancy may prefer to stay at a low valence state, which will affect their activity in the DE process. Based on the above analysis, we can understand why the $\rho - \delta$ relation is nonlinear. As for the exponential variation of ρ against δ, its physical origin remains to be revealed.

For the curves below 200 K, there is a visible upturn at $\delta \sim 0.077$, which interrupts the exponential variation of resistivity. It is likely a consequence of the reduction of hole concentration. Mott et al. [20] has investigated the conduction of a system with random potential fluctuation, and suggested the presence of minimum conductivity at the transition from an extended state to a localized state: $\sigma_{\min} \sim 600/a\ \Omega^{-1}\text{cm}^{-1} \approx 150\ \Omega^{-1}\text{cm}^{-1}$, where a is the lattice constant and it is ∼4 Å for the manganites. Extrapolating the $\rho(T)$ relation of LSMO to 0 K, we obtained $\sigma \approx 257\ \Omega^{-1}\text{cm}^{-1}$ and $42\ \Omega^{-1}\text{cm}^{-1}$ respectively for $\delta = 0.055$ and 0.077. These values are very near the minimum conductivity. Therefore, it is possible that charge localization occurs in the low temperature region for $\delta > 0.077$, causing the rapid resistivity increase. A similar but more drastic resistivity increase is also observed in LaSr [16,17]. According to Yamada et al. [21], polaron ordering takes place in the low temperature region below a critical x, which localizes the conduction electrons. The resistive upturn in LSMO film may have a similar origin. It is interesting to note that the resistivity of the LSMO films is smaller than that of LaSr for $x < 0.17$, which is presumably a result that the polaron ordering in the former is not perfect due to the presence of lattice defects. Therefore, the behavior of the LSMO film is

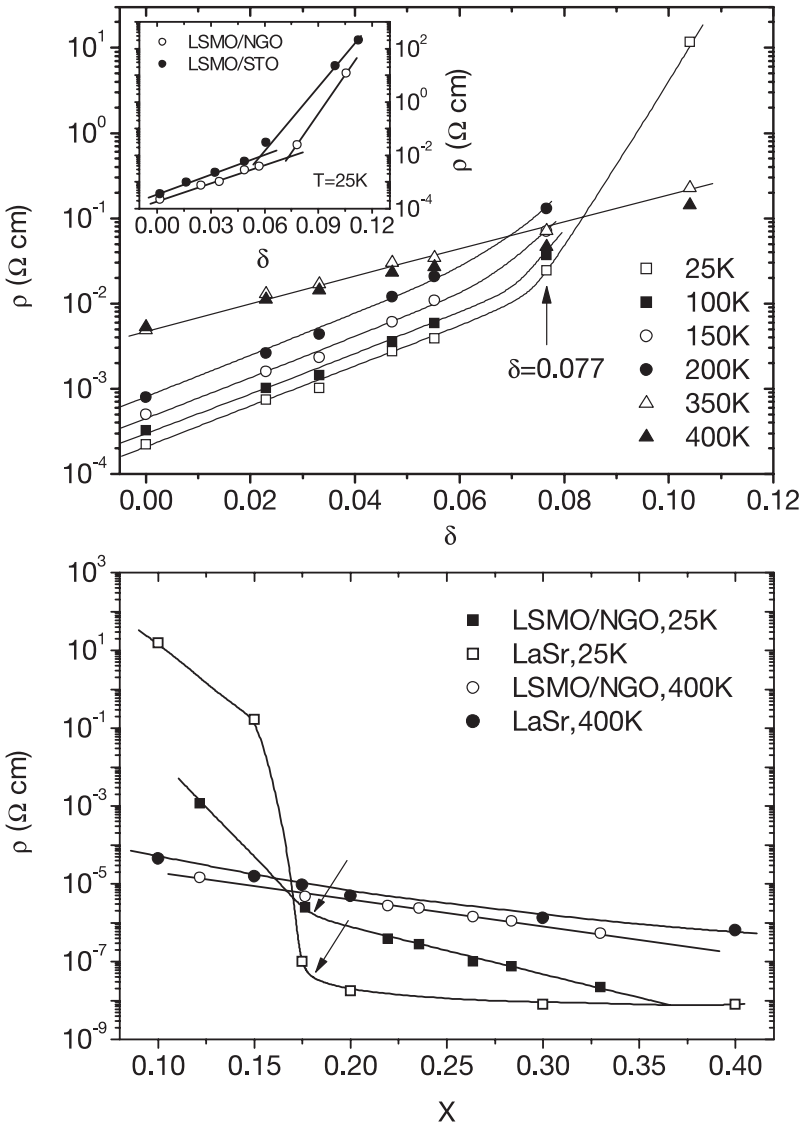

Fig. 6. Resistivity as a function of the concentration of oxygen vacancies (top panel) or holes (bottom). Data for the $La_{1-x}Sr_xMnO_3$ single crystals (LaSr) are extracted from reference [16].

miscellaneously determined by the variation of the content of Mn^{4+} and the vacancy scattering to the DE. The former is more important in the low temperature region.

Differences between the film and the crystal are not significant in the temperature region above ∼350 K. As shown in Figure 6 (bottom panel), the ρ (400 K)$-\delta$ curves of the LSMO films and the LaSr crystals coincides with each other fairly well though the minor deviation from the exponential variation of the latter, and there are no any anomalies around x ∼0.18. Similar phenomenon is observed at $T = 350$ K. All these results reveal the insensitivity of the semiconducting conduction to lattice defects. According to the previous work, the conduction above T_p is dominated by the hopping of small polarons between Mn ions [22,23]. In this case, the scattering by misaligned spins and the trapping by $Mn^{3+}O_6^{2-}$ octahedra (Jahn-Teller distortion) [24] of the e_g electrons play a dominative role, while the scattering of anionic vacancies may act as an unimportant perturbation when their content is not larger.

Another interesting issue is the temperature dependence of resistivity, which involves the mechanism influencing the transport process. Generally, people fit the $\rho(T)$ relation by [25–27]

$$\rho = \rho_0 + \alpha T^2 + \beta T^{9/2}. \quad (1)$$

The first term is residual resistivity, the second term corresponds to a single-magnon process, its presence has been discussed by Jaime et al. [25], and the third term to a two-magnon process [28]. Figure 7 shows the prototypical results of curve-fitting for selected samples. The insets show the difference between the measured and calculated data. An excellent fitting is obtained in a wide temperature region below T_p when δ is small. For δ=0,

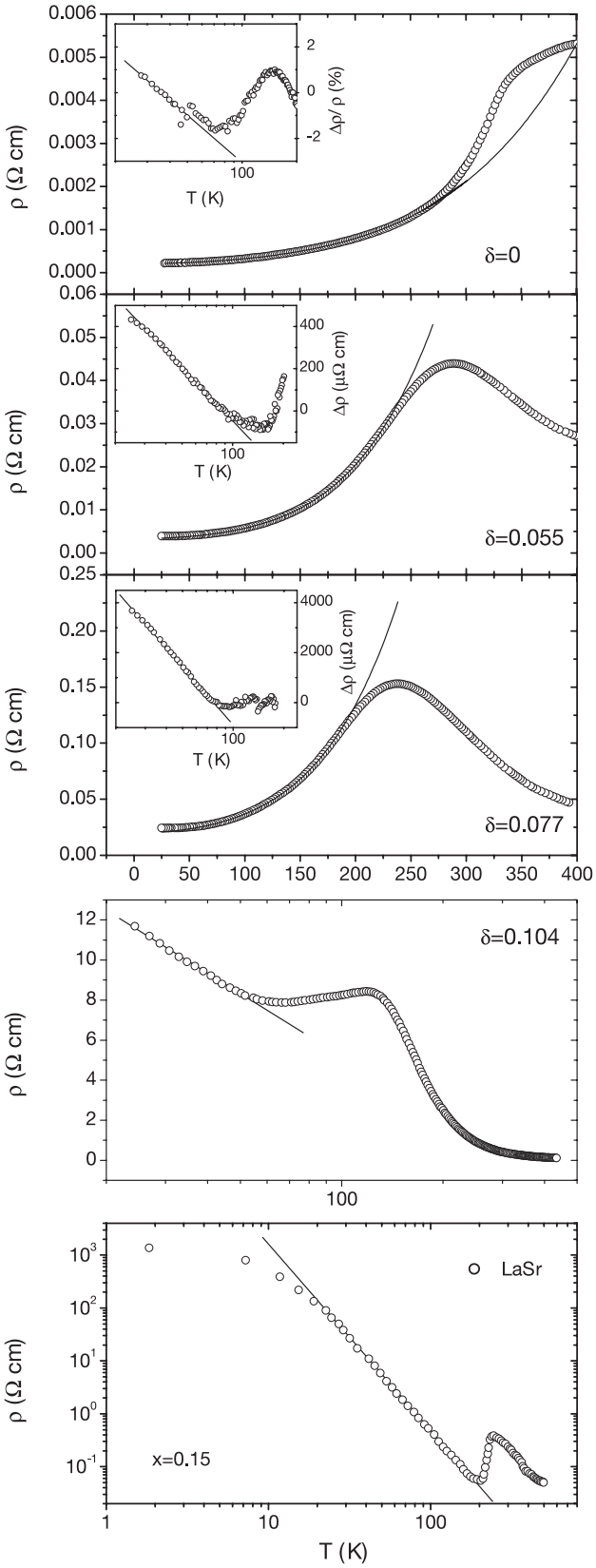

Fig. 7. Observed (symbols) and calculated (solid lines) resistivity. Results of $La_{1-x}Sr_x$- MnO_3 ($x = 0.15$) are presented in the bottom panel. The insets display the difference between the curve-fitted and measured data.

Table 1. Concentration of oxygen vacancies, fitted parameters, and the critical temperature for the M-I transition for LSMO/NGO.

δ	T_p (K)	α ($\Omega\,\mathrm{cm\,K^{-2}}$)	β ($\Omega\,\mathrm{cm\,K^{-4}}$)	γ (Ω cm)/ lnK
0	355	2.09×10^{-4}	1.1×10^{-10}	
0.023	338.4	7.68×10^{-4}	2.0×10^{-10}	
0.033	329.7	1.04×10^{-3}	3.2×10^{-10}	
0.047	308	1.90×10^{-3}	9.1×10^{-10}	
0.055	288	3.32×10^{-3}	2.0×10^{-9}	1.008
0.077	238.2	1.97×10^{-2}	1.5×10^{-8}	8.343
0.104	120			34.297
0.118	0			45445.6

the relative difference between the fitted and measured data is smaller than 1% when the fitting parameters $\rho_0 = 2 \times 10^{-4}\ \Omega\,\mathrm{cm}$, $\alpha = 1.1\times10^{-8}\ \Omega\,\mathrm{cm\,K^{-2}}$, and $\beta = 6.5 \times 10^{-15}\ \Omega\,\mathrm{cm\,K^{-9/2}}$ are used. These are parameters reasonably consistent with those obtained by Okuda et al. [17] for LaSr ($\rho_0 = 0.8 \times 10^{-4}\ \Omega\,\mathrm{cm}$ and $\alpha = 0.67 \times 10^{-8}\ \Omega\,\mathrm{cm\,K^{-2}}$), Jaime et al. [25] for $La_{0.67}(Pb,Ca)_{0.33}MnO_3$ ($\rho_0 = 1.3\times10^{-4}\ \Omega\,\mathrm{cm}$ and $\alpha = 1.28\times10^{-8}\ \Omega\,\mathrm{cm\,K^{-2}}$) and Zhao et al. [26] for $La_{0.75}Ca_{0.25}MnO_3$ ($\beta = 12\times10^{-15}\ \Omega\,\mathrm{cm\,K^{-9/2}}$). With the progress of oxygen release, the fitting remains quite well, while the fitting parameter increases rapidly (Tab. 1). To clarify the variation of the fitting parameters with oxygen deficiency, in Figure 8 we show the $\alpha - x$ dependence. Results of LaSr are also presented for comparison. Obviously, α increases against x more rapidly in the LSMO films. According to Jaime et al. $\alpha \propto 1/(k_F^5 D^2)$, where k_F represents the Fermi wave vector and D the stiffness of spin waves. It is obvious that both the reduction in x and the increase in δ will depress k_F and D. Therefore, the magnon-electron interaction in oxygen-deficient films is stronger compared to the LaSr with similar hole content.

It is obvious that the low temperature resistivity upturn in the $\rho(T)$ curves for $\delta > 0.077$ can not be described by equation (1). A careful analysis indicates that the deviation from equation (1) emerges even when δ is small, and can be described by a new term of the form $-\ln(T)$, which is particularly apparent in the case of $\delta = 0.104$ ($x = 0.125$). For a manganite with a perfect ferromagnetic order, the magnetic scattering of the e_g electrons could be negligibly small according to the DE theory. However, the lattice defects in oxygen-deficient films may weaken the ferromagnetic coupling between Mn ions, producing an inhomogeneous magnetic structure. It is possible that deviations from the ferromagnetic spin alignment occur first near oxygen vacancies, which act as centers for magnetic scattering and lead to the Kondo-effect-like behavior. We also investigated the $\rho(T)$ relation of LaSr ($x = 0.15$), and found a different relation $\rho \propto T^{-3.52}$.

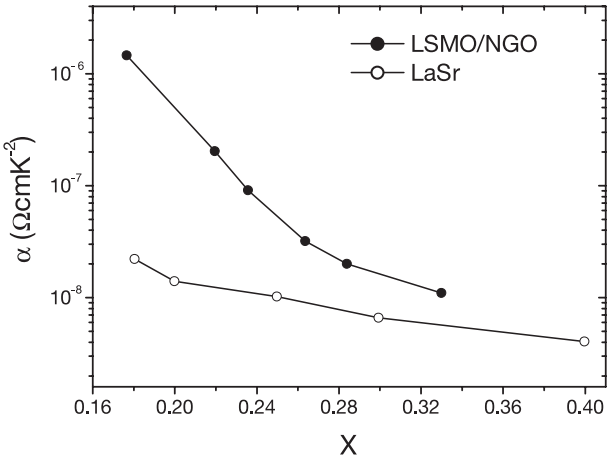

Fig. 8. Parameter of curve-fitting as a function of hole concentration. Results for the single crystal $La_{1-x}Sr_xMnO_3$ are also presented.

3.3 Metal-to-insulator transition

As is well known, electronic transport enhances at T_c for the manganites because of the ferromagnetic alignment of the core spins of the Mn ions, which favors charge exchange. Generally, T_p coincides with T_c and, therefore, is a convenient measure of the magnetic coupling between Mn ions. In Figure 9 we show the variation of T_p with the content of oxygen vacancies. T_p locates respectively near ∼355 K and ∼348 K in the oxygen stoichiometric LSMO/NGO and LSMO/STO. It is slightly lower in the latter, which may be a consequence of tensile strain. Oxygen losing causes a monotonic decrease of T_p. The $T_p - \delta$ curve is relatively flat when δ is small, and the variation of T_p speeds up gradually with the increase of δ. T_p decreases only by 25 K when δ increases from 0 to 0.03, while ΔT_p is ∼44 K for the next increment of $\Delta\delta \sim 0.03$. No M-I transition can be identified when $\delta > 0.104$ for LSMO/NGO and δ>0.08 for LSMO/STO. Similar phenomena are observed in the LCMO films except for that the $T_p - \delta$ relation is linear when δ is not too large (This could be a common feature of the LCMO system because similar behavior appears in the films on different substrates.)

There are reports about the effects of the content of Mn^{4+} on T_p [16,29]. The top inset of Figure 9 is a comparison of the normalized T_p's of the LSMO films and the LaSr crystals, depicted as functions of x. The overall tendency is very similar for the films and the crystals, which suggests the predominant role of the Mn^{4+} concentration. This is different from what occurring in the low temperature region, where the vacancy scattering governs the transport process.

However, differences in the detailed features of the $T_p - x$ curves do exist for the three systems. First, though the two curves for LSMO/NGO and LaSr coincide with each other quite well in the range $x = 0.2 - 0.33$, discrepancy appears and develops below $x = 0.2$. At $x = 0.14$, difference in T_p can be as large as ∼32% (corresponding to ∼50 K noting that the T_p for the as-prepared film

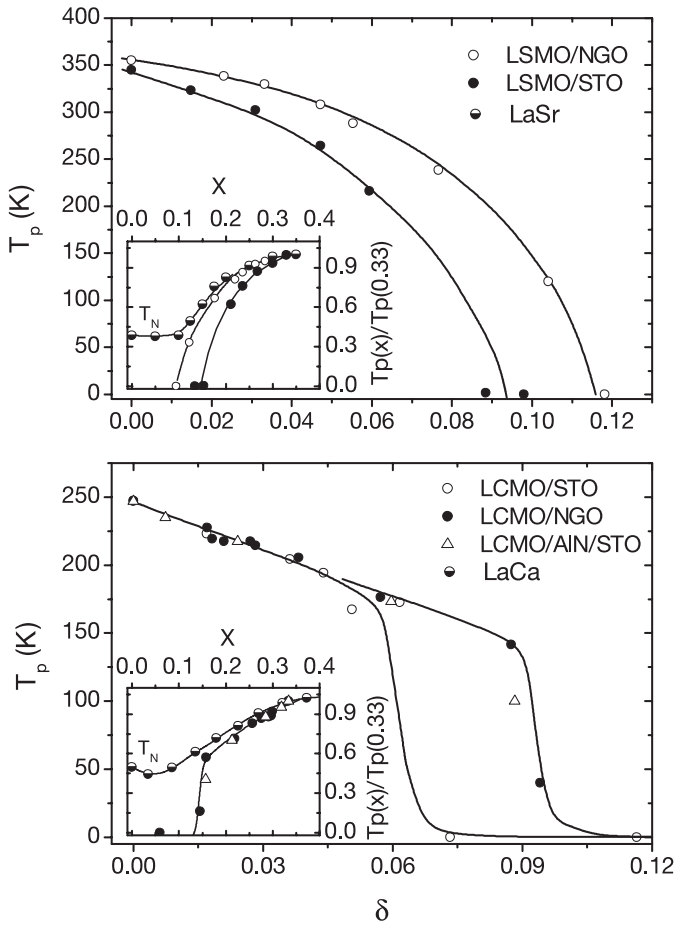

Fig. 9. Critical temperature for the metal-to-insulator transition (T_p) as a function of the content of oxygen vacancies. Top and bottom panels correspond to the LSMO films and the LCMO films, respectively. The inset presents a comparison to the results of the corresponding crystals. LaSr (data from Ref. [16]) and LaCa (data from Ref. [24]) represent $La_{1-x}Sr_xMnO_3$ and $La_{1-x}Ca_xMnO_3$, respectively. LCMO/AlN/STO denotes the LCMO film on STO with a AlN buffer layer.

is ∼355 K at $x = 0.33$). Second, T_p varies with δ more rapidly in LSMO/STO than in LSMO/NGO. The difference in T_p of the two films is ∼10 K for $\delta = 0$ and ∼70 K for $\delta = 0.06$. As a consequence, the critical oxygen content for the disappearance of the M-I transition is different for the two films, and the $\Delta\delta$ can be as large as ∼0.023. This may be a common feature of the vacuum-annealed films for that a similar phenomenon is observed in LCMO. In that case, the difference of the critical δ is ∼0.031 (bottom panel of Fig. 9).

It has been proved that one percent Ga can cause a decrease in T_p of ∼12 K [30]. If the effects due to the vacancy scattering are more or less the same, an extra reduction of ∼50 K of T_p for 4% oxygen vacancies ($\delta = 0.12$) is expected. In Figure 10 we show the excessive change of T_p of LSMO/NGO, obtained by simply subtracting the two sets of T_p's of LSMO/NGO and LaSr with the same

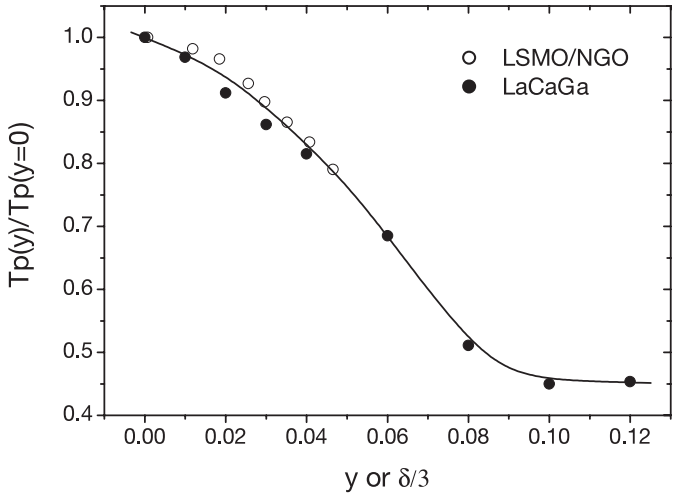

Fig. 10. Reduced T_p against the content of oxygen vacancies for LSMO/NGO and the content of Ga for $La_{0.67}Ca_{0.33}Mn_{1-y}Ga_yO_3$ (LaCaGa) (data from Ref. [30]).

x values. T_p of the $La_{0.67}Ca_{0.33}Mn_{1-y}Ga_yO_3$ compounds is also presented, as a function of y, for comparison. The general features of the $T_p - x$ and $T_p - \delta/3$ curves are quite similar ($\delta/3$ is used considering the fact that there are three oxygen anions in each perovskite unit cell). This result proves that the discrepancy between the LSMO films and LaSr crystals is due to the scattering of oxygen vacancies.

The difference in the critical δ values for the films on STO and NGO may be a consequence of the fact that the strains in the films are different. It is generally believed that a compressive stress will drive T_p to higher temperatures, while a tensile stress depresses T_p [31]. The strain effects may become stronger as the hole concentration decreases (or δ increases). As reported by Chen et al. [32], the change in T_c can be as large as ∼50% when the strain in the $La_{0.9}Sr_{0.1}MnO_3$ film changes. With this in mind, the increase of ΔT_p with δ and the different critical δ's in the two films are readily understood. T_p is lower in LSMO/STO is also consistent with the observation that the resistivity of this film is higher compared with LSMO/NGO (inset in Fig. 6).

4 Summary

Effects of oxygen content on the transport behavior of epitaxial $La_{2/3}Sr_{1/3}MnO_{3-\delta}$ films on (110) $NdGaO_3$ and (001) $SrTiO_3$ substrates have been experimentally studied. The oxygen release, measured by the change of lattice parameter, can be controlled by annealing the film at different temperatures in vacuum. It is found that oxygen escapes at similar rate for the two films despite their different strains and crystal qualities. Oxygen nonstoichiometry causes a monotonic decrease of the critical temperature for the metal-to-insulator transition (T_p), and a quantitative relation between T_p and δ is established. A comparison to crystals $La_{1-x}Sr_xMnO_3$ indicates that the reduction of hole concentration due to the incorporation of anionic vacancies dominates the variation of T_p, while the vacancies themselves influence the detailed features of the T_p-δ dependence. Strain in the film affects the effects of oxygen deficiency, and the metal-to-insulator transition disappears at a smaller δ value in the tensily stressed film. Similar phenomena are observed in $La_{0.67}Ca_{0.33}MnO_{3-\delta}$ films. In the temperature region above T_p, oxygen vacancies affect the resistive behavior of the films mainly by modulating the content of Mn^{4+}. In contrast, the extra effects due to the scattering of oxygen vacancies become important in the low temperatures region, and cause an exponential increase of resistivity with δ. A further analysis indicates that magnon-electron scattering determines the low temperature resistivity. Oxygen deficiency enhances this scattering significantly, and a resistivity upturn of the form $-\ln(T)$ can be resulted when δ exceeds 0.05.

This work was supported by the National Natural Science Foundation of China, the State Key Project for Fundamental Research of China, and by a Direct Grant from the Research Grants Council of the Hong Kong Special Administrative Region, China (Project No. C001-2060228).

References

1. For a review, see *Colossal Magnetoresistance, Charge ordering, and Related Properties of manganese Oxides*, edited by C.N.R. Rao, B. Raveau (World Scientific, Singapore, 1998); *Colossal Magnetoresistance Oxides*, edited by Y. Tokura (Gordon & Breach, London, 1999)
2. C. Zener, Phys. Rev. **82**, 403 (1955); P.W. Anderson, H. Hasegawa, Phys. Rev. **100**, 675 (1955)
3. G.H. Jonker, J.H. Van Santen, Physica **16**, 337 (1950); **19**, 120 (1955)
4. H.L. Yakel, Acta Cryst. **8**, 394 (1955); E.D. Wollan, W.C. Koehler, Phys. Rev. **100**, 545 (1955)
5. J.F. Mitchell, D.N. Argyriou, C.D. Potter, D.G. Hinks, J.D. Jorgensen, S.D. Bader, Phys. Rev. B **54**, 6172 (1996)
6. Q. Huang, A. Santoro, J.W. Lynn, R.W. Erwin, J.A. Borchers, J.L. Peng, K. Ghosh, R.L. Greene, Phys. Rev. B **58**, 2684 (1998)
7. H.L. Ju, J. Gopalakrishnan, J.L. Peng, Q. Li, G.C. Xiong, T. Venkatesan, R.L. Greene, Phys. Rev. B **51**, 6143 (1995)
8. A.M. De Léon-Guevara, P. Berthet, J. Berthon, F. Millot, A. Revcolevschi, A. Anane, C. Dupas, K. Le Dang, J.P. Renard, P. Veillet, Phys. Rev. B **56**, 6031 (1997)
9. K.M. Krishnan, H.L. Ju, Phys. Rev. B **60**, 14793 (1999)
10. J.-M. Liu, Q. Huang, J. Li, C.K. Ong, Z.C. Wu, Z.G. Liu, Y.W. Du, Phys. Rev. B **62**, 8976 (2000)
11. J.R. Sun, G.H. Rao, B.G. Shen, H.K. Wong, Appl. Phys. Lett. **73**, 2998 (1998); J.R. Sun, B.G. Shen, H.W. Yeung, H.K. Wong, J. Phys. D: Appl. Phys. **35**, 173 (2002)
12. L. Malavasi, M.C. Mozzati, C.B. Azzoni, G. Chiodelli, G. Flor, Solid State Commun. **123**, 321 (2002)
13. R. Shiozaki, K. Takenaka, Y. Sawaki, S. Sugai, Phys. Rev. B **63**, 184419 (2001)
14. X.T. Zeng, H.K. Wong, Appl. Phys. Lett. **66**, 3371 (1995)
15. R.D. Shannon, Acta Cryst. A **32**, 751 (1976)

16. A. Urushibara, Y. Moritomo, T. Arima, A. Asamitsu, G. Kido, Y. Tokura, Phys. Rev. B **51**, 14103 (1995)
17. T. Okuda, A. Asamitsu, Y. Tomioka, T. Kimura, Y. Taguchi, Y. Tokura, Phys. Rev. Lett. **81**, 3203 (1998)
18. C. Kittel, *Introduction to Solid State Physics*, 5th edn. (John Wiley & Sons, Inc. 1976)
19. J.L. Alonso, L.A. Fernandez, F. Guinea, V. Laliena, V. Martin-Mayor, Phys. Rev. B **66**, 104430 (2002)
20. N.F. Mott, E.A. Davis, *Electronic Processes in Non-crystalline Solids*, 2nd edn. (Oxford University Press, Now York, 1979)
21. Y. Yamada, O. Hino, S. Nohdo, R. Kanao, T. Inami, S. Katano, Phys. Rev. Lett. **77**, 904 (1996)
22. N. Noginova, G.B. Loutts, E.S. Gillman, V.A. Atsarkin, A.A. Verevkin, Phys. Rev. B **63**, 174414 (2001)
23. P.S. Anil, Kumar, P.A. Joy, S.K. Date, J. Phys.: Condens. Matter **10**, L269 (1998)
24. A.J. Millis, Nature **392**, 147 (1998)
25. M. Jaime, P. Lin, M.B. Salamon, P.D. Han, Phys. Rev. B **58**, R5901 (91998)
26. G.M. Zhao, D.J. Kang, W. Prellier, M. Rajeswari, H. Keller, T. Venkatesan, R.L. Greene, Phys. Rev. B **63**, 060402 (2000)
27. G.M. Zhao, H. Keller, W. Prellier, D.J. Kang, Phys. Rev. B **63**, 172411 (2001)
28. K. Kubo, N. Ohata, J. Phys. Soc. Jpn **33**, 21 (1972)
29. H. Fujishiro, M. Ikebe, Y. Konno, J. Phys. Soc. Jpn **67**, 1799 (1998)
30. J.R. Sun et al. (unpublished)
31. T.Y. Koo, S.H. Park, K.B. Lee, Y.H. Jeong, Appl. Phys. Lett. **71**, 977 (1997); R.A. Rao, P.D. Lavric, T.K. Nath, C.B. Eom, Appl. Phys. Lett. **73**, 3294 (1998)
32. X.J. Chen, S. Soltan, H. Zhang, H.-U. Habermeier, Phys. Rev. B **65**, 174402 (2002)